A cell-free therapy for articular cartilage repair based on synergistic delivery of SDF-1 & KGN with HA injectable scaffold

Wu, Huachu ; Shen, Liang ; Zhu , Zhu ; Luo, Xusong ; Zhai, Yishu ; Hua, Xiaobin ; Zhao, Shicheng ; Cen, Lian ; Zhang, Zhibing

DOI:
10.1016/j.cej.2020.124649

Document Version
Peer reviewed version

Citation for published version (Harvard):
Wu, H, Shen, L, Zhu , Z, Luo, X, Zhai, Y, Hua, X, Zhao, S, Cen, L & Zhang, Z 2020, 'A cell-free therapy for articular cartilage repair based on synergistic delivery of SDF-1 & KGN with HA injectable scaffold', *Chemical Engineering Journal*, vol. 393, 124649. https://doi.org/10.1016/j.cej.2020.124649

A Cell-free Therapy for Articular Cartilage Repair Based on Synergistic Delivery of SDF-1 & KGN with HA Injectable Scaffold

Huachu Wu[1#], Liang Shen[1#], Zhu Zhu[2], Xusong Luo[2],Yishu Zhai[1], Xiaobin Hua[1], Shicheng Zhao[1], Lian Cen[1], Zhibing Zhang[3]**

[1]Shanghai Key Laboratory of Multiphase Materials Chemical Engineering, Department of Product Engineering, School of Chemical Engineering, East China University of Science and Technology. No.130 Mei Long Road, Shanghai, 200237, China.

[2]Department of Plastic and Reconstructive Surgery, Shanghai 9th People's Hospital, Shanghai Jiaotong University School of Medicine, Shanghai, 200011, China.

[3]School of Chemical Engineering, University of Birmingham, Edgbaston, Birmingham B15 2TT, UK.

[#]These authors contributed equally to this work.

Running title: Co-encapsulation of SDF-1 & KGN within individual microsphere for synergistic cartilage repair

***** To whom correspondence should be addressed.

Tel: +86-21-64252808; Fax: +86-21-64253159.

E-mail: Prof. Lian Cen: liancen@ecust.edu.cn

Prof. Zhibing Zhang: z.zhang@bham.ac.uk

Abstract

This study was to co-encapsulate a chemokine (stromal cell-derived factor-1, SDF-1) and a chondroinductive molecule (kartogenin, KGN) within microspheres via microfluidics, and to incorporate them into a hyaluronic acid (HA) injectable scaffold for articular cartilage defect repair. HA injectable scaffold, as a cartilage-friendly microenvironment, was prepared by crosslinking HA with 1,4-butanediol diglycidyl ether. A microfluidic device was set up to prepare monodisperse PLGA microspheres (49 μm) to load SDF-1 and KGN. An in vivo model of full-thickness articular cartilage defects in rabbits was applied to evaluate the reparative capacity of the current package. The SDF-1 and KGN were co-encapsulated simultaneously within the core and shell area of the microsphere with high loading efficiency and sustained release profiles of more than 2 months. The release profiles of them were highly matched and well fitted to a first-order mathematical model. These microspheres when incorporated into HA injectable scaffold were demonstrated to heal the full-thickness articular cartilage defects in rabbits. The regenerated tissue had the typical cartilage histological characters and integrated well with the surrounding tissue at 12w. This developed cell-free system could serve as an efficient therapy for articular cartilage defects treatment, serving as a supplementary way to cell based therapies.

Keywords: co-encapsulation, SDF-1, KGN, cartilage regeneration, injectable scaffold

1. Introduction

Articular cartilage is a thin hydrated tissue which covers articulating surfaces. Mature articular cartilage is avascular and the articular chondrocytes are highly differentiated cells that have seriously limited self-repair capacity.[1] Moreover, untreated cartilage defects often progress to osteoarthritis.[1,2] Hence, there has been continuing efforts on developing regenerative medicine strategies to repair full thickness articular cartilage defects.[1,3] Stem cell-based therapy and autologous chondrocyte implantation (ACI) have been demonstrated promising in repairing articular cartilage defects.[1,3-6] However, in case of no autologous chondrocytes or stem cells available, it is necessary to develop alternative therapy based on well-defined biomaterials and drugs. It is thus proposed in the current study to co-encapsulate chemokines (e.g. stromal cell-derived factor-1, SDF1) and small chondroinductive molecules (e.g. kartogenin, KGN) within biodegradable core-shell microspheres to be generated using microfluidic technology, which can be subsequently incorporated into pre-established crosslinked hyaluronic acid (HA) injectable scaffolds for articular cartilage defect repair.

The efficiency of co-encapsulation largely depends on the preparation methods of microspheres. Poly(lactide-co-glycolide) (PLGA) were often used as original materials for microspheres due to their favorable biocompatibility and biodegradability.[7,8] Traditionally, micro-/nano- particles of these materials are fabricated through an emulsification-based process which is limited in leeway to adjust the drug payload and tune the versatile formulation of two or more active ingredients to be delivered. Moreover, the resulting micro-/nano- particles have polydisperse sizes.[9] In contrast, recently developed microfluidic technology allows the production of monodisperse microspheres with high

encapsulation efficiency, the precise control of the payload and the core-shell ratio of microspheres.[10-12] Hence, a microfluidic technology would be adopted to prepare PLGA microspheres with core-shell structure to load a chemokine and a chondroinductive molecule simultaneously within one microsphere. This proposed microencapsulation strategy could thereby enhance the loading efficiency of these molecules, while the microspheres could also serve as sites for cell homing and tissue regeneration with a long lasting efficacy.

As to the chemokines to be encapsulated, SDF- 1 would be a superior choice. It is a cytokine that belongs to the CXC class of chemokine proteins and the only known natural chemokine in the body that is activated by binding to CXCR4 receptors which are expressed by hematopoietic stem cells, endothelial progenitor cells, mesenchymal stem cells (MSCs) and the like.[13,14] The SDF1/CXCR4 complex was shown to play a key role in stem cell homing.[15] It is well established that potentially useful cell populations already exist in the body and attracting these cells to a desired anatomic site by cell homing to promote endogenous regeneration offers new therapeutic options.[16] In case of disease or injury, the endogenous stem/progenitor cells would migrate to and engraft in the affected tissue, then proliferate extensively and differentiate specifically. However, when such innate reparative or self-repair system is not sufficient, it is necessary to introduce additional signals which would instruct the recruitment of more endogenous stem cells to the target site and activation of regeneration.[16] Such strategy was proved to be promising for clinical translation because it avoids extensive ex vivo cell culture.[17] However, its success depends on first identifying the bioactive macromolecules that mediate tissue-specific homing and then manipulating the homing cells to initiate the repair/regeneration process. KGN, a small molecular organic compound, identified recently to induce

the bone marrow-derived mesenchymal stem cells (BMSCs) into chondrocytes, can stimulate runt-related transcription factor (RUNX) family members, mainly RUNX1 expression, which is important in chondrogenesis, chondrocyte proliferation, and survival.[1] Our proposed microspheres would serve as a smart package that could not only sustain the release of SDF-1 for a long duration, but also could manipulate the chondrogenic differentiation of the homed cells by simultaneously releasing KGN (instead of additional in vitro chondrogenesis step).

The current work was thus to use microfluidic technology to prepare core-shell PLGA microspheres loaded with SDF-1 and KGN (within the core and shell, respectively) for their sustained release to repair articular cartilage defects, when incorporated into HA injectable scaffolds. The hydrogel network of our HA injectable scaffolds was previously demonstrated to provide a superior and favorable microenvironment for cartilage regeneration.[18] A capillary-based microfluidic device was designed to prepare homogeneous and monodisperse PLGA microspheres to load SDF-1 and KGN. The morphological and structural characters of these microspheres were then explored, and the loading capacity as well as release profiles was evaluated via mathematical models. An in vivo model of full-thickness articular cartilage defects in rabbits was then applied to evaluate the cartilage reparative capacity of the current developed cell-free system with a follow-up of 12w. A synergistic cell homing and chondrogenesis within a cartilage friendly microenvironment could thus be expected from such a system, which could efficiently serve as an alternative and necessary supplementary therapy for articular cartilage defect treatments.

2. Materials and methods

2.1 Materials

Poly(lactide-co-glycolide) (PLGA, Purasorb® PDLG 5010) was supplied by Purac Biomaterials Company Inc (Holland). Poly(vinyl alcohol) (PVA, Mw:13,000-23,000, 87-89% hydrolyzed), Nile-Red and 1,4-Butanediol diglycidyl ether (BDDE) were purchased from Sigma-Aldrich (USA). Methylene blue hydrate was supplied by Macklin Biochemical Co., Ltd. (Shanghai, China). Dichloromethane (DCM) (analytical grade) was obtained from Shanghai Chemical Reagent Co., Ltd (China). SDF-1 was purchased from Peprotech (USA) and KGN was obtained from Sigma-Aladdin (USA). Hyaluronic acid sodium salt (HA, MW: 1.5×10^6 Da) was obtained from Shandong Freda Biopharm Co., Ltd. (Jinan, China). All other chemicals and reagents were used as received without further processing and of analytical grade unless otherwise specified.

2.2 Preparation of HA injectable scaffold

HA injectable scaffolds were fabricated by crosslinking HA with BDDE as reported in our previous work.[18] In brief, HA (10 wt%) was first dissolved in 1% NaOH solution. After HA complete dissolution, BDDE (0.4 vol%) was added to the HA solution with vigorous stirring. The solution was then crosslinked at 40°C for 5 h followed by being dried at ambient temperature for 3 days. After that, the dried HA was swollen by adding sufficient phosphate buffered saline (PBS: NaCl, 9 mg /mL; KH_2PO_4, 0.03 mg/mL; $Na_2HPO_4{\cdot}2H_2O$, 0.14 mg/mL; pH=7). The resulting HA hydrogel was placed in a dialysis bag and dialyzed with excess deionized (DI) water and PBS to remove residual BDDE. The HA hydrogel, with HA content of 20 mg/ mL, was then smashed with a homogenizer (T10 basic, IKA, Germany) to obtain gel particles of 0–400μm as the HA injectable scaffolds (without free water

outside the gel). The gel particles were elastic and in the solid state as demonstrated previously.[18] Before being used for the in vivo injection, HA injectable scaffolds were sterilized in a high-pressure steam sterilizer set at 120^{o}C for 20 min.

2.3 Preparation of PLGA microspheres

A glass capillary microfluidic device,[19,20] was first assembled using two round glass capillaries inserted into a square glass capillary (1mm x 1mm) from the opposing direction as illustrated in Figure 1. Briefly, three syringe needles were glued over one end of a round glass capillary and two ends of the square glass tube, and they were used as connectors for the innermost water phase, middle oil and outer water phases, respectively. The other exposed end of the round glass capillary was served as the sample collection tube. The orifice diameter of the innermost phase of the device (D_o) was 100 μm, and the diameter of the collection tube tip of the device was 300 μm. W/O/W double emulsion droplets were then prepared using this device. To prepare KGN and SDF-1 loaded PLGA microspheres, PLGA of 79.6 mg was dissolved in 10 mL of DCM as the solution A, and KGN of 5 mg was dissolved in 3.1512 ml of DMSO as the solution B. The solution B of 204.1 μl was added to the solution A to form the middle oil phase of W/O/W emulsions, which was injected into the interstice between the square capillary and the round tube. SDF-1 aqueous solution (20 μg/ml) was used as the innermost phase of W/O/W emulsions flowing through the tapered round glass capillary. The PVA aqueous solution (2 wt%) pumped through the square capillary from the opposite direction of the inner and middle phase was acted as the outermost water phase. The volume flow rates of innermost water (Q_i), middle oil (Q_m) and outer water phases (Q_o) were typically set to be 1000, 2000, and 6000 μL/h, respectively, controlled respectively by syringe pumps (Harvard Apparatus Pump11 Elite, USA). Drug-loaded

PLGA emulsion droplets were formed in the sample collection capillary, and collected using PVA aqueous solution (0.5 wt%) in a glass beaker. These droplets were ultimately solidified by evaporation of DCM at ambient temperature under constant stirring (280 rpm, 24 h), and PLGA microspheres were collected by centrifugation (5,000 rpm, 5 min, Beckman Coulter, USA). The microspheres need to be washed for five times with de-ionized water to remove PVA residue, and then freeze-dried using a freeze dryer (12 h, YB-FD-1, Shanghai, China). To facilitate the in vitro measurement of release profiles of drugs loaded within PLGA microspheres prepared by using the current microfluidic method, Nile-Red (NR, oil-soluble) and Methylene blue hydrate (MB, water-soluble) were used as model drugs to represent the above KGN and SDF-1, respectively. Hence, the same operation and parameters were applied except the replacement of KGN with NR and SDF-1 with MB.

2.4 Determination of drug loading and encapsulation efficiency

The drug loading and encapsulation efficiency was determined according to a previous reported method.[21] Briefly, dried PLGA microspheres of 5 mg were dissolved in 1 ml of DCM for 10 min and 5 ml of 10% isopropanol in phosphate buffered saline (PBS, pH 7.4, Sigma-Aldrich, USA) was then added for 30 min. The mixture was vigorously shaken for 2 min in order to extract NR and MB into 10% isopropanol PBS mixture solution. After centrifuging, the aqueous solution was withdrawn, the NR and MB content of the solution was determined by UV-VIS spectrophotometer (UV2550, SHIMADZU, Japan) at absorbance of 554 nm and 664 nm, respectively, according to their respective calibration curves. This study was performed in triplicate. The encapsulation efficiency (EE) was then determined by the equation:

$$\mathrm{EE}(\%) = \frac{M_R}{M_T} \times 100\%$$

Where M_R is the actual mass of NR or MB determined in the microspheres (measured value) and M_T is the total mass of NR or MB used for preparing the microcapsules (theoretical value). The drug loading (DL) was calculated from:

$$\mathrm{DL}(\%) = \frac{M_R}{M_P} \times 100\%$$

Where M_P is the total mass of microspheres. The analyses were carried out using samples of triplicate runs, and the results were expressed as mean ± SD (n = 3).

2.5 Characterizations of PLGA microspheres

The surface and cross-sectional morphology of the obtained PLGA microspheres was observed by Field-emission scanning electron microscopy (Tokyo, Japan). The size and size distribution were determined by measuring 200 microspheres in the SEM images with Nano Measurer software. The coefficient of variation (CV) of the PLGA microspheres was then calculated from the statistical data based on the following equation:[22]

$$\mathrm{CV} = \frac{\sigma}{D_p}$$

Where σ is the standard deviation of the diameter (μm) and D_p is the mean diameter (μm). Confocal scanning laser microscopy (CSLM, Leica TCS sp8) was further used to observe the distribution of MB and NR (core and shell, respectively) within the PLGA microspheres (NR: 488 nm; MB: 405 nm).

2.6 In vitro release property

The freeze-dried microspheres loaded with NR and MB were immersed in 5 mL of PBS solution (10% isopropanol, 0.1% Tween 80) in 10 mL disposable sterile polypropylene centrifuge tubes at 37ºC in an incubator (Thermo., USA). At predetermined time intervals, the sample tubes were taken out from the incubator and centrifuged (6000 rpm, 10min, Beckman Coulter, USA). After centrifugation,

supernatant (3 mL) was withdrawn for measurement by UV-VIS spectrophotometer (UV2550, SHIMADZU, Japan) at absorbances of 554 nm (NR) and 664 nm (MB), respectively, according to their respective calibration curves. Each sample was repeated in triplicate. Fresh PBS solution of 3 mL (10% isopropanol，0.1% Tween 80) was supplemented to the sample tube before being back to the incubator.

2.7 In vivo articular cartilage repair

To test the in vivo efficacy of the HA injectable scaffold integrated with PLGA microspheres loaded with KGN and SDF-1, the New Zealand White rabbits (2.7−3.0 kg, 5−6 months old) were utilized as the animal model. All the animal procedures were approved by the Animal Care and Experiment Committee of School of Medicine, Shanghai JiaoTong University. The full-thickness cartilage defects (3.5 mm in diameter, 3.0 mm in depth) were created in the center of the trochlear groove by a drill as described previously and a subsequent standard microfracture procedure was performed.[1,23,24] The amount of sample used for filling the defect was 0.03 ml by injecting via a syringe. The sample was prepared by mixing 1 ml HA injectable scaffolds with 53 mg PLGA microspheres (with or without SDF-1&KGN) via pipetting; or 1ml HA injectable scaffolds alone. Rabbits were randomly assigned into four groups: defects treated with HA injectable scaffolds with SDF-1 and KGN loaded PLGA microspheres (HA/PLGA/SDF-1/KGN, n=3 at each time point); defects treated with HA injectable scaffolds with PLGA microspheres (HA/PLGA group, n=3 at each time point); defects treated with HA injectable scaffolds (HA group, n=3 at each time point); defects left untreated (Control group, n=3 at each time point). The animals were allowed to have free movements in their cages after surgery. The limbs were allowed to bear the whole weight. General health status was monitored by a

veterinarian. The rabbits were euthanized at 8 and 12 weeks post-surgery for sample harvest, respectively. Subsequently, various evaluations were performed to estimate the cartilage regeneration.

2.8 Macroscopic evaluation

The regenerated tissue was assessed using the International Cartilage Repair Society (ICRS) (shown in Table S1 of the Supporting Information) macroscopic score, which contains three categories: degree of defect repair; integration to board zone; and macroscopic appearance.[25] The scoring was performed by three different investigators.

2.9 Histological observation

The harvested samples were fixed in 10% formalin for 7 days and then decalcified in 15% EDTA for 4 weeks in a shaker at room temperature with the solution changed twice a week. After this, the samples were transferred to 4% Paraformaldehyde Fix Solution for 24 h, dehydrated, and embedded in paraffin. After being embedded in paraffin, the samples were cut into sections of 5 μm. The sections were then stained with hematoxylin-eosin (H&E) and toluidine blue (TBO) to examine the histological morphology. Observation was performed under a light microscope (NIKON ECLIPSE E100, Japan). The repaired tissue was graded by three different investigators, using the ICRS visual histological assessment scale (shown in Table S2 of the Supporting Information).[26] For immunohistochemical evaluation, primary antibodies, rabbit anti-collagen II antibody (dilution ratio=1:200, Bioss, Germany) were used in the present study. Biotinylated secondary HRP-labeled Goat Anti-Rabbit IgG (H+L) (dilution ratio=1:1, DAKO) was used. The tissue sections were first placed in a repair kit filled with citrate antigen repair buffer (PH 6.0) for 1 h at 37 °C for antigen retrieval. The sections were placed in 3% H_2O_2 (Hydrogen peroxide: pure water = 1:9) to block endogenous peroxidase, and 3% BSA (Sigma)

was used to block nonspecific protein binding. After overnight incubation with primary antibody at 4 °C, the sections were incubated with the secondary antibody for 50 min at room temperature. The DAB substrate system was used to develop the color. Microscopic observation was then carried out on these slides.

2.10 Statistical Analyses

All results were expressed as mean ± standard deviation (SD). All experiments were repeated for three times. Student t-tests were used to determine statistical significance between groups, and $p<0.05$ was considered significant.

3. Results and discussion

3.1 HA injectable scaffolds

The feasibility of using homogenized HA hydrogel as an injectable scaffold has been demonstrated in our previous work.[18] As briefly illustrated in Figure 2, HA hydrogels were prepared first by crosslinking HA with BDDE. The formed bulk hydrogel was then homogenized into irregular micro-hydrogel of 0-400μm in size, which could be then used simply by injection as an injectable scaffold. Biological species, such as growth factors or cells could be physically mixed with this scaffold to be delivered into tissues.

3.2 Morphological and structural characters of PLGA microspheres

According to the FESEM images of the obtained PLGA microspheres as shown in Figure 3A, they were spherical in size with a highly monodisperse and well dispersion without any aggregation. The statistical analysis of the diameter of these microspheres was analyzed using Nano Measurer software based on the respective SEM images (Figure 3B). It was shown that the mean diameter of PLGA microspheres prepared under the current fixed conditions was 49 μm (n=200). Microspheres of 46-51 μm in diameter accounted for ~95% of the total. Accordingly, CV of the PLGA microspheres was 3.83%, indicating a narrow size distribution.

CSLM observation was carried out on the PLGA microspheres loaded with NR and MB, which were supplemented at the middle oil phase (the PLGA layer) and at the innermost water phase, respectively. Three dimensional CLSM views of the PLGA microspheres were shown in Figure 3C. It can then be seen that the light intensity of NR was mainly enriched in the outer layer of the PLGA microsphere (Figure 3D), while that of MB was mainly enriched in the innermost layer of the microsphere (Figure

3E). From the above image information, it could also be ascertained that a little amount of NR was also distributed in the innermost space of PLGA microspheres. Vice verse, a trace amount of MB could also be located in the outer layer of PLGA microspheres. The cross-sectional morphology of these microspheres was further characterized by FESEM as shown in Figure 3F. It was surprised to see that the PLGA microspheres were not hollow in structure and a highly porous inner structure was observed with a relatively thick outer layer structure. Probably, the porous structure could make room for the efficient encapsulation of water soluble drugs, while the thickness of the outer PLGA layer could actually be controlled by the variation of operation parameters, such as the relative flow rates of water and oil phases as well as the device geometry of microfluidics to efficiently regulate the relative amounts of the oil-soluble drug and the water-soluble drug.

According to previous reports, physical parameters, such as nano-/micron-scale internal structures, surface morphology, and size distributions are critical, in that they can play an important role in the control of loading efficiency, release kinetics and biological activities of the encapsulated substances.[27] Usually, optimal release profiles are achieved by using microspheres with diameters in the range of 10-200 μm,[28,29] as there is a risk that microspheres will be phagocytosed by immune cells for particle diameters < 10 μm and microspheres > 200 μm may cause an immune response and inflammation.[30] Therefore, the uniform and reproducible PLGA microspheres in the range of 46-51 μm prepared by our microfluidic technique were suitable as drug carriers and also as a component of an injectable system in our current work to treat articular cartilage defects.

The current fabricated PLGA microspheres have the dimpled surface as demonstrated previously.[31] The advantage of a dimpled surface or golf-ball feature lies in the increased surface area for drug

release, and provision of additional loading sites on the particle surface for further interaction with biological systems.[27,32] As to our work, the microspheres would act as both a depository for sustained release of biomolecules and the anchoring points for substantially homed cells, in such case the enhanced surface area with biological systems would be desirable.

In addition, as shown in Figure 3F, the interior of the obtained PLGA microspheres has a honeycomb inner structure, probably due to the instability of the inner phase water/oil emulsion, which on the other hand facilitates the distribution and adhesion of water-soluble drugs. As shown in CLSM image of Figure 3E, the blue dyes were enriched especially around those honeycomb surfaces. The pattern of blue dyes was in consistent with the pattern of inner pore distribution as shown in the cross-sectional morphology.

3.3 In vitro release profile of drug loaded PLGA microspheres

The in vitro release profiles of encapsulated drugs within PLGA microspheres were evaluated by choosing MB as a water-soluble drug model encapsulated with the inner water phase and NR as an oil-soluble drug model embedded with intermediate PLGA oil phase. The reason why we preferred to use MB and NR to address the in vitro release behavior of PLGA microspheres was mainly the economic cause as all of these tests would consume large amounts of these two biomolecules. The second reason was the well-established quantitative method for MB and NR, which is easy and quick to acquire and consequently could reduce the operational errors usually occurred during drug concentration determination.

The EE of NR, located mainly in the outer layer of PLGA microspheres as shown in Figure 3D was determined to be 96.08%, while the EE of MB located mainly in the inner layer of PLGA microspheres

was determined to be 97.04%. Moreover, DL was found to be 0.07% for NR and 0.61% for MB, respectively. The reason why DL was pre-set to be very low was mainly to take full consideration of the reported viable KGN value of 100 mM shown to be effective on chondrocytes,[24] and this was also the case for the specificity of SDF-1.[13,16] Moreover, it also has to be mentioned that the DL of drug loaded PLGA microcapsules could be further increased by the increase in the drug concentration used in the middle oil phase and the inner water phase, respectively. In addition, our current study is to construct co-encapsulation of SDF-1 and KGN within microspheres for synergistic delivery to treat articular cartilage defects. The main function of SDF-1 is cell homing, and SDF-1 works by binding to cell surface receptor, CXCR4, which are expressed by hematopoietic stem cells, endothelial progenitor cells, MSCs and the like.[13-15] KGN induces chondrogenesis, chondrocyte proliferation, and survival.[3] The individual function of them might not be expected to regenerate articular cartilage fully. The advantage of current co-encapsulation is proposed that with the release of SDF-1, BMSCs could be expected to be recruited from marrow clot created during the microfracture procedure to the site where the microspheres are located. This site could also release KGN at the same time, which could then induce the homed BMSCs to differentiate into chondrocytes. In addition, the whole system, most probably, might also recruit synovium-derived mesenchymal stem cells from synovial membrane, and chondrocytes from surrounding healthy cartilage. If they were separately embedded, it would be very difficult to achieve the synergistic effect of these two drugs since it was difficult to match them spatio-temporally.

The corresponding release profiles of drugs from the PLGA microcapsules were shown in Figure 4. The cumulative release percentages of the NR and MB were leveled off upon 70 and 60 days,

respectively. The release pattern of NR could be divided into two stages: the stage one was round 0-30 d with a relatively fast release rate and a NR cumulative release of 71%; the second one was around 30-70 d, where the release rate slowed down and the NR cumulative release reached around the maximum of around 96% as an almost constant platform. In addition, the release pattern of MB could be divided roughly into three stages: the first stage was round 0-10d, which was featured with a slow release rate and had a MB cumulative release of less than 10%; the second stage was 10-30 d, which had a relatively fast release rate and a MB cumulative release of around 70%; and the third one was 30-60 d, where the release rate decreased obviously compared to the second stage and finally a MB cumulative release percent of around 96% was reached.

NR, as an oil-soluble model drug, was located mainly in the outer layer of PLGA microsphere, which might account for its relatively earlier release over MB during the first month of the whole release period. MB, as a water-soluble model drug mainly located within the porous area in the core of PLGA microspheres, was released slowly at the first 30 d, then almost released at the same rate as NR from 30 d to 50 d, and later reached the plateau around 10 days earlier than NR. It was reasonable to observe that MB would be a little lag behind initially since its diffusion would be more hindered by the outer PLGA layer. With the progress of hydrolysis and progress of NR release, MB diffusion would be significantly enhanced with time. As an indication from the above phenomenon, KGN would thus release faster than SDF-1 at the first month, while from 30d to around 50 d KGN and SDF-1 could have the matched release rates.

These two drugs were almost synchronized from the beginning to the 60th day of release, which was of high importance in the current design package that later needs the synergy of KGN and SDF-1

within a HA based reservoir microenvironment. Moreover, during the whole release period, no burst release was noticed either on NR or MB, and both of them had gradual increase in the released amounts. The little variation among the samples was also another feature of the microspheres prepared via microfluidic technology.

Hydrolysis mediated degradation of PLGA was one of the main factors controlling the whole release duration. Another important factor was the diffusion which was in turn affected by the hydrophilic property and local concentration of model drugs, and the porosity of microspheres. It would be difficult to identify at each of the above distinct period which factor dominated the release of each drug since hydrolysis was also not a uniformly progressed but highly dynamic process.[33] Last but not of lease to mention was the regulation that could be gained by adjusting the flow rate ratio of the internal aqueous phase and the intermediate oil phase, and the drug concentration, to change the shell thickness and drug loading of the PLGA microsphere.

3.4 Drug release kinetics

In order to gain more understanding on the drug release behavior and mechanism as well, the results of the above in vitro drug release profile (Figure 4) over a period of 80 d were fitted to various mathematical models. Zero order model, first order models, the Higuchi model and Korsmeyer-Peppas modelswere evaluated.[34-37] For the zero-order model, the release rate is given by the following equation:

$$\frac{M_t}{M_R} = kt$$

In which Mt is the amount of drug released at time t, k is the zero-order release constant, and M_R is the amount of the total drug in the sample.

A first-order release rate can be described by the following equation:

$$\frac{M_t}{M_R} = \exp(-kt)$$

In which k is the first-order release constant.

A model developed by Higuchi is presented by the following equation:

$$\frac{M_t}{M_R} = kt^{(1/2)}$$

Where k is the Higuchi release rate.

The Korsmeyer-Peppas model can be described by the following equation:

$$\frac{M_t}{M_R} = kt^n$$

Where k is the Korsmeyer-Peppas constant and n is the release exponent which is dimensionless.

The results of regression analysis, R^2, were applied to correlate the fit to different models as summarized in Table 1. On the basis of best fit with the highest correlation (R^2) value, it is concluded that the in vitro release profiles of MB and NR could be best expressed by the first order equation, due to their highest R^2 (MB: R^2=0.959, NR: R^2=0.995), followed by Higuchi model (MB: R^2=0.940, NR: R^2=0.963) and Korsmeyer-Peppas model (MB: R^2=0.920, NR: R^2=0.952) with zero order model as the poorest fit.

NR, with a molecular weight of 318.37 was used to represent KGN which had a close molecular weight of 317.37. Hence, KGN release kinetics could also be well correlated by the above first order model which had a high regression value of 0.995. The later stage of in vivo study to optimize the dosage effect of KGN could be better facilitated through referring to this fitted model by reducing the number of experimental trials. It has been well established that several processes contribute to the overall

kinetics of drug release from PLGA microspheres including chemical degradation of the polymer by ester hydrolysis, polymer erosion, evolution of pore structure as a result of mass erosion and diffusive transport of the drug through the polymer matrix and the aqueous pore structure.[8] The term degradation usually refers to the process through which the polymer chain bonds are hydrolyzed to form oligomers and monomers, while the term erosion refers to the loss of mass due to diffusion of water-soluble, small oligomers and monomers out of the polymer matrix.[8,38] The drug release kinetics is actually the dynamic and case-specific coupling between these three processes. In most cases, drug release in PLGA microspheres were classified as being erosion-controlled,[8] which could be further specified as surface-eroding or bulk-eroding. PLGA microspheres (10s to 100s of microns) are being eroding controlled since the hydration time scale is on the order of a few minutes compared to weeks or months for degradation.[39,40] The release of hydrophobic drugs, in the current work, NR or KGN, would most probably diffuse through the PLGA matrix and dissolute coincident with polymer dissolution and/or erosion. This diffusion and dissolution became slowed down upon 30 days on, most probably due to the more dominant role of polymer degradation at this time.

SDF-1, with a molecular weight of around 8K Da, has a certain degree of difference when being modeled with MB of 319.85. The best fitting among the models tried in this work was also the first order one. For highly water-soluble drugs and macromolecular drugs such as proteins or peptides, diffusion through the aqueous pores is a more important model of transport than their diffusion through the PLGA matrix which is initially more hydrophobic. This could help to account for the few days of initial lag of MB. As the pore network develops, the effective diffusivity of MB enhanced and the period of 10-30 days could thus experience such effect with the driving force being more concentration

dominated. The difference of MB and SDF-1 would probably have a relatively significant effect on their initial diffusion through PLGA polymer matrix, whereas the diffusion through the pore network could neglect such difference. Despite of this difference in molecular weight, this kinetic modeling by using MB could still be a valid correlation with SDF-1 release as reviewed by Braatz and Abidian about the previous mentioned general processes during drug release. [8,41] However, a more sophisticated model would still be necessary with more factors being addressed, such as the current core-shell structure, the diameter of the microspheres and the concentration of each drug.

3.5 Articular cartilage defects repair in rabbits

3.5.1 Gross evaluation

At the pre-defined time points of 8 and 12 weeks, the rabbits were sacrificed, and the femoral condyles of all four groups were harvested as displayed in Figure 5. As shown in Figure 5A1, the HA/PLGA/SDF-1/KGN group exhibited a remarkable filling of the articular cartilage defect at 8w. At 12w, the defects became so difficult to distinguish as a nice filling with smooth and whitish appearance was achieved as shown in Figure 5A2. It seems that a nice interface with excellent healing was achieved between the regenerated tissue and its adjacent native cartilage (Figure 5A2). In contrast to reparative conditions of the experimental group, the defects in the HA/PLGA and HA groups were occupied with new regenerated tissue but still with an obvious scar-like appearance (Figure 5B1 and B2 & Figure 5C1 and C2). Moreover, the defect of the control group which was left un-repaired, remained empty with the collapse of its adjacent cartilage tissue (Figure 5D1 and D2). The corresponding ICRS macroscopic grading including degree of defect repair, integration to border zone, macroscopic appearance and overall repair assessment were performed to evaluate the repaired

condition of each group as shown in Figure 5B and C. Obviously, the macroscopic scores obtained from the experimental group (HA/PLGA/SDF-1/KGN) were statistically better than those in other groups (all macroscopic appearance of the experimental group (HA/PLGA/SDF-1/KGN) at 12 w is shown in Figure S2 of the Supporting Information). The HA/PLGA/ SDF-1/KGN group got the highest ICRS macroscopic scores of 19.7 ± 0.9 and 23.7 ± 0.5, which were 4.6 ($p<0.001$) and 5.9 ($p< 0.001$) folds of the respective ones of the Control group at 8 and 12 weeks, respectively. Moreover, the ICRS macroscopic scores of HA/PLGA group were 15.7 ± 0.9 and 15.1 ± 0.8, which were 3.7 ($p<0.001$) and 3.8 ($p<0.001$) folds of the respective ones of the Control group at 8 and 12 weeks, respectively. The HA group was scored 12 ± 0.8 and 12.7 ± 0.5, which were 2.8 ($p<0.001$) and 3.2 ($p<0.001$) folds of the respective ones of the Control group at 8 and 12 weeks, respectively. The Control group exhibited the least ICRS macroscopic scores of 4.3 ± 0.5 and 4 ± 0.8 at 8 and 12 weeks, respectively.

Based on the above observation and scores, it could be indicated that the repair condition of HA/PLGA/SDF-1/KGN group was enhanced with time as the scores increased with time ($p< 0.05$). However, the repair conditions of other groups were all almost constant as no difference was observed on their scores over time. Moreover, HA/PLGA and HA groups also achieved some degree of tissue repair, indicating a favorable microenvironment provided by HA hydrogels.

3.5.2 Histological analyses of regenerated cartilages

The histological analyses of different groups of regenerated cartilage-like tissues were presented in Figure 6. As shown in Figure 6A1, the defects of the HA/PLGA/SDF-1/KGN group were repaired by newly generated tissue featured with lacunas and cell clusters, a typical histological character of cartilage tissue, and the engineered cartilage-like tissue integrated well with its adjacent cartilage and

its underlying subchondral bone at 8w. At 12w, the surface and thickness of engineered cartilage was more even, and it seems that the engineered cartilage became more mature. The neo-tissue was characterized with a similar cartilage thickness to those of the surrounding native cartilage tissue and had been fully integrated with the native one and the subchondral bone as shown in Figure 6A2. However, only localized cartilage tissue could be identified in the defect of HA/PLGA group and some of the defect area was filled with fibrous tissue. The integrity of the subchondral bone was not remained (Figure 6B1). The repair condition of the same group was even worsened with time as shown in Figure 6B2. As to the defect of HA group at 8w, the repair condition was quite good as the defect was filled with mostly neo-cartilage-like tissue except that at the center of the defects, degradation of the subcondral bone could be identified (Figure 6C1). However, the reparative condition of HA group deteriorated over time as most of the defect area became fibrous tissue filled as shown Figure 6C2. Moreover, the defect of the control group got even worse over those of the HA/PLGA and HA groups at 8w (Figure 6D1), and terrible collapse of the subcondral bone occurred at 12 w (Figure 6D2). According to the high-magnification H&E images of the repaired tissue at the central area as shown in Figure 6B, the HA/PLGA/SDF-1/KGN group not only had the typical structures of lacunas and cell clusters, but exhibited zonal articular cartilage structure as those of normal ones. However, the others are all fibrous ones (Figure 6B). According to the high-magnification H&E images of the repaired tissue at the interface (Figure 6C), the HA/PLGA/SDF-1/KGN group still exhibited minor defects at 8 w and further remodeled with time to become more even.

The corresponding ICRS visual histological evaluation of surface, matrix, subchondral bone and cartilage mineralization were performed to evaluate and compare the reparative conditions of each

group as shown in Figure 6D and E. Obviously, the visual histological scores obtained from the experimental group (HA/PLGA/SDF-1/KGN) were statistically higher than those in other groups. The HA/PLGA/SDF-1/KGN group got the highest scores of 11.3 ± 0.5 and 11.7 ± 0.5, which were 16.1 ($p<0.001$) and 39 ($p<0.001$) folds of the respective ones of the Control group at 8 and 12 weeks, respectively. Moreover, the ICRS visual histological scores of HA/PLGA group were 4 ± 0.8 and 2.3 ± 0.5, which were 5.7 ($p<0.001$) and 7.7 ($p<0.001$) folds of the respective ones of the Control group at 8 and 12 weeks, respectively. The HA group was scored 7.3 ± 0.5 and 1.7 ± 0.5, which were 10.4 ($p<0.001$) and 5.7 ($p<0.001$) folds of the respective ones of the Control group at 8 and 12 weeks, respectively. The Control group exhibited the least ICRS visual histological scores of 0.7 ± 0.5 and 0.3 ± 0.5 at 8 and 12 weeks, respectively. The above histological morphology of the engineered tissue further confirmed but more clearly revealed the reparative conditions observed by macroscopic observation conditions of each group. It could also be clear that a cartilage-friendly microenvironment provided by HA hydrogel itself was important to initiate a favorable repair but was not enough to sustain a durable one since with time the defects became either degraded or more fibrous tissue dominated. Biological molecules of sustained effect thus could help to compensate the necessary effects which prevented the degradation of the initiated repair process.

3.5.3 Expression of cartilage specific ECM

Deposition of glycosaminoglycan (GAG) in the engineered cartilage tissue was confirmed by TBO staining at 8w and 12w post-surgery (Figure 7), respectively. GAG deposition was intensively observed in the HA/PLGA/SDF-1/KGN group (Figure 7A1), which further enhanced with time to show a more even and continuous layer of new cartilage tissue (Figure 7A2). However, almost no

GAG deposition or weak GAG staining was observed in the defect area of other groups either at 8 w or 12 w (Figure 7 B1,B2; C1,C2; D1,D2), respectively. Expression of COL II in the engineered cartilage was further revealed by immunohistochemical staining as shown in Figure 8. The COL II expression profile with time of each group was in well consistence with that of GAG deposition. That is, cartilage matrix production was more abundant in the defect area of the HA/PLGA/SDF-1/KGN group and became more homogenous and mature with time.

It is also important to mention that collagen type I staining could be carried in the future. Factors that might contribute to collagen type I expression are mainly the differentiation status of recruited cells and the fibrosis phenomena of the degenerated fibrocartilaginous or regenerated cartilaginous tissue of the defect. It was reported that with the protection effect of KGN, the fibrosis effect was minimized and chondrogenic differentiation of BMSCs or synovium-derived mesenchymal stem cells could be enhanced.[3,23,24] The collagen type I would thus be weakened significantly with the effect of KGN, while the collagen type II would be enhanced in turn, which was proven by both in vitro and in vivo works.[24] Moreover, it was speculated that the collagen type I and type II would be more distinctly expressed by different groups and would also progress in different ways with time.

Although it was demonstrated that the above package including HA injectable scaffold and SDF-1 & KGN co-encapsulated microspheres was effective in treating articular cartilage defects in rabbits, there are still a few issues left to be further addressed. We still need a longer follow-up to give a more substantial evaluation that the neo-tissue would not undergo fibrous degradation which is usually the case for a few current clinical therapies, such as microfracture. Whether there is room for further adjusting the current dosage of SDF-1 and KGN would also be informative at the end of a prolonged

follow-up. On the other hand, it was only shown here that the neo-tissue bore great similarity to the histology of the normal articular cartilage tissue. Further confirmation at the molecular biology level remains to be carried out, which could help to identify the homed cells, trace their origin, and explore the quantitative correlation among SDF-1, KGN and cell status.

Moreover, it was speculated that the in vitro synergetic effect of SDF-1 and KGN on chondrogenic differentiation of stem cells might be investigated in the future through cell migration assays. As reported, the in vitro individual effect of SDF-1 has been demonstrated to induce cell migration using a transwell migration model.[42] The in vitro effect of KGN on stem cells was shown to promote chondrocyte differentiation from MSCs under both monolayer and high-density culture conditions.[3] It might be possible that in addition to monitor the cell migration, the cell differentiating condition could also be evaluated when systems with both SDF-1 and KGN were designed. It was thus further speculated that SDF-1 could promote the in vitro MSCs migration, while KGN could promote chondrocyte differentiation from the migrated MSCs. Future work would be necessary to ascertain this.

HA injectable scaffold is also an indispensible component of this design package. It not only provides a cartilage-friendly microenvironment, but also helps to stabilize the microspheres within the defect area instead of being flowing away. It further helps to stabilize the homed cells. The HA scaffold alone was not enough to initiate a sustainable repairing process as shown in the control group. Our previous work confirmed its role as an injectable scaffold [18]. That is, it not only acted as a delivery vehicle and also facilitated the morphogenesis as a three-dimensional hydrogel scaffold by working as tissue filler and augmenting volume. As a scaffold for cells, its primary role appeared to be retention of cells, thereby facilitating the expected biological repair processes and morphogenesis. Moreover, the

degradation of this injectable scaffold could be tuned by the microenvironment, the presence of cells and cell physiological states. That is, cells or extracellular matrix within this scaffold could easily help to adjust its turnover, probably due to the biological nature of HA.

However, although this is only a preliminary study to show a viable and promising articular cartilage therapy, the novelty still stands that this is the first to use microfluidic technology to achieve a controllable co-encapsulation and co-release of SDF-1 and KGN to expect a relatively precise way of articular cartilage regeneration.

4. Conclusion

SDF-1 and KGN was co-encapsulated successfully within the core and shell area of PLGA microspheres facilitated by the current microfluidic technology. They had a matchable sustained release to expect a synergistic functioning process, that is, KGN provides protection and desired induction on the SDF-1 mediated homing cells. These microspheres together with HA injectable scaffold was demonstrated to heal the full-thickness articular cartilage defects in rabbits. The current developed system could well expect a synergistic cell homing and chondrogenesis within a cartilage friendly microenvironment, which could be efficiently used to repair articular cartilage defects in case of no desired cells available, serving as an alternative and necessary supplementary therapy.

Acknowledgement

This study is financially supported by National “973” Project Foundation (2010CB944804) and Newton Research Collaboration award from The Royal Academy of Engineering.

Conflict of Interest

The authors declare no conflict of interest.

References:

[1] E. A. Makris, A. H. Gomoll, K. N. Malizos, J. C. Hu, K. A. Athanasiou, Repair and tissue engineering techniques for articular cartilage, Nat. Rev. Rheumatol. 11 (2015) 21-34.

[2] J. W. Bijlsma, F. Berenbaum, F. P. Lafeber, Osteoarthritis: an update with relevance for clinical practice, Lancet 377 (2011) 2115–2126.

[3] K. Johnson, S. Zhu, M. S. Tremblay, J. N. Payette, J. Wang, L. C. Bouchez, S. Meeusen, A. Althage, C. Y. Cho, X. Wu, P. G. Schultz, A stem cell-based approach to cartilage repair, Science 336 (2012) 717-721.

[4] M. Brittberg, A. Lindahl, A. Nilsson, C. Ohlsson, O. Isaksson, L. Peterson, Treatment of deep cartilage defects in the knee with autologous chondrocyte transplantation, N. Engl. J. Med. 331 (1994) 889-895.

[5] B. Johnstone, M. J. Stoddart, G. I. Im, Multi‐disciplinary approaches for cell‐based cartilage regeneration, J. Orthop Res. (2019) doi: 10.1002/jor.24458.

[6] F. Zeifang, D. Oberle, C. Nierhoff, W. Richter, B. Moradi, H. Schmitt, Autologous chondrocyte implantation using the original periosteum-cover technique versus matrix-associated autologous chondrocyte implantation: a randomized clinical trial, Am. J. Sports. Med. 38 (2010) 924-933.

[7] I. Bala, S. Hariharan, M. N. Kumar, PLGA nanoparticles in drug delivery: the state of the art, Crit. Rev. Ther. Drug Carrier. Syst. 21 (2004) 387-422.

[8] A. N. Ford Versypt, D. W. Pack, R. D. Braatz, Mathematical modeling of drug delivery from autocatalytically degradable PLGA microspheres--a review, J. Control. Release 165 (2013) 29-37.

[9] S. Freitas, H. P. Merkle, B. Gander, Microencapsulation by solvent extraction/evaporation: reviewing the state of the art of microsphere preparation process technology, J. Control. Release 102 (2005) 313-332.

[10] G. M. Whitesides, The origins and the future of microfluidics, Nature 442 (2006) 368-373.

[11] M. A. Zieringer, N. J. Carroll, A. Abbaspourrad, S. A. Koehler, D. A. Weitz, Microcapsules for enhanced cargo retention and diversity, Small 11 (2015) 2903-2909.

[12] S. S. Datta, A. Abbaspourrad, E. Amstad, J. Fan, S. H. Kim, M. Romanowsky, H. C. Shum, B. Sun, A. S. Utada, M. Windbergs, S. Zhou, D. A. Weitz, 25th anniversary article: double emulsion templated solid microcapsules: mechanics and controlled release, Adv. Mater. 26 (2014) 2205-2218.

[13] K. Hattori, B. Heissig, K. Tashiro, T. Honjo, M. Tateno, J. H. Shieh, N. R. Hackett, M. S. Quitoriano, R. G. Crystal, S. Rafii, M. A. Moore, Plasma elevation of stromal cell-derived factor-1 induces mobilization of mature and immature hematopoietic progenitor and stem cells, Blood 97 (2001) 3354-3360.

[14] E. Lagasse, H. Connors, M. Al-Dhalimy, M. Reitsma, M. Dohse, L. Osborne, X. Wang, M. Finegold, I. L. Weissman, M. Grompe, Purified hematopoietic stem cells can differentiate into hepatocytes in vivo, Nat. Med. 6 (2000) 1229-1234.

[15] D. Seol, D. J. McCabe, H. Choe, H. Zheng, Y. Yu, K. Jang, M. W. Walter, A. D. Lehman, L. Ding, J. A. Buckwalter, J. A. Martin, Chondrogenic progenitor cells respond to cartilage injury, Arthritis. Rheum. 64 (2012) 3626-3637.

[16] Y. Yu, M. J. Brouillette, D. Seol, H. Zheng, J. A. Buckwalter, J. A. Martin, Use of recombinant human stromal cell-derived factor 1α-loaded fibrin/hyaluronic acid hydrogel networks to achieve

functional repair of full-thickness bovine articular cartilage via homing of chondrogenic progenitor cells, Arthritis. Rheum. 67 (2015) 1274-1285.

[17] W. Shen, J. Chen, T. Zhu, L. Chen, W. Zhang, Z. Fang, B. C. Heng, Z. Yin, X. Chen, J. Ji, W. Chen, H. W. Ouyang, Intra-articular injection of human meniscus stem/progenitor cells promotes meniscus regeneration and ameliorates osteoarthritis through stromal cell-derived factor-1/CXCR4-mediated homing, Stem Cells Transl. Med. 3 (2014) 387-394.

[18] R. Yang, L. Tan, L. Cen, Z. Zhang, An injectable scaffold based on crosslinked hyaluronic acid gel for tissue regeneration, RSC Adv. 6 (2016) 16838-16850.

[19] W. J. Duncanson, T. Lin, A. R. Abate, S. Seiffert, R. K. Shahe, D. A. Weitz, Microfluidic synthesis of advanced microparticles for encapsulation and controlled release, Lab. Chip 12 (2012) 2135-2145.

[20] R. K. Shah, H. C. Shum, A. C. Rowat, D. Lee, J. J. Agresti, A. S. Utada, L. Y. Chu, J. W. Kim, A. Fernandez-Nieves, C. J. Martinez, Designer emulsions using microfluidics, Mater. Today 11 (2008) 18-27.

[21] Y. Y. Yang, T. S. Chung, N. P. Ng, Morphology, drug distribution, and in vitro release profiles of biodegradable polymeric microspheres containing protein fabricated by double-emulsion solvent extraction/evaporation method, Biomaterials 22 (2001) 231-241.

[22] S. W. Choi, Y. Zhang, Y. Xia, Fabrication of Microbeads with a Controllable Hollow Interior and Porous Wall Using a Capillary Fluidic Device, Adv. Funct. Mater. 19 (2009) 2943-2949.

[23] X. Li, J. Ding, Z. Zhang, M. Yang, J. Yu, J. Wang, F. Chang, X. Chen, Kartogenin-Incorporated Thermogel Supports Stem Cells for Significant Cartilage Regeneration, ACS Appl. Mater.

Interfaces 8 (2016) 5148-5159.

[24] D. Shi, X. Xu, Y. Ye, K. Song, Y. Cheng, J. Di, Q. Hu, J. Li, H. Ju, Q. Jiang, Z. Gu, Photo-Cross-Linked Scaffold with Kartogenin-Encapsulated Nanoparticles for Cartilage Regeneration, ACS Nano 10 (2016) 1292-1299.

[25] M. P. van den Borne, N. J. Raijmakers, J. Vanlauwe, J. Victor, S. N. de Jong, J. Bellemans, D. B. Saris, International Cartilage Repair Society (ICRS) and Oswestry macroscopic cartilage evaluation scores validated for use in Autologous Chondrocyte Implantation (ACI) and microfracture 1, Osteoarthr. Cartilage 15 (2007) 1397-1402.

[26] P. Mainil-Varlet, T. Aigner, M. Brittberg, P. Bullough, A. Hollander, E. Hunziker, R. Kandel, S. Nehrer, K. Pritzker, S. Roberts, E. Stauffer, Histological assessment of cartilage repair: a report by the Histology Endpoint Committee of the International Cartilage Repair Society (ICRS), J. Bone Joint Surg. AM. 85-A (2003) 45-57.

[27] K. H. Hwangbo, M. R. Kim, C. S. Lee, K. Y. Cho, Facile fabrication of uniform golf-ball-shaped microparticles from various polymers, Soft Matter 7 (2011) 10874-10878.

[28] F. Y. Han, K. J. Thurecht, A. K. Whittaker, M. T. Smith, Bioerodable PLGA-Based Microparticles for Producing Sustained-Release Drug Formulations and Strategies for Improving Drug Loading, Front. Pharmacol. 7 (2016) 185.

[29] M. S. Shive, J. M. Anderson, Biodegradation and biocompatibility of PLA and PLGA microspheres, Adv. Drug Deliv. Rev. 28 (1997) 5-24.

[30] G. J. Dawes, L. E. Fratila-Apachitei, K. Mulia, I. Apachitei, G. J. Witkamp, J. Duszczyk, Size effect of PLGA spheres on drug loading efficiency and release profiles, J. Mater. Sci. Mater. Med.

20 (2009) 1089-1094.

[31] H. Chen, F. Jia, C. Zhu, J. Xu, X. Hua, Z. Xi, L. Shen, S. Zhao, L. Cen, Controllable preparation of SB-3CT loaded PLGA microcapsules for traumatic-brain-injury pharmaco-therapy, Chem. Eng. J. 339 (2018) 346-358.

[32] M. R. Kim, S. Lee, J. K. Park, K. Y. Cho, Golf ball-shaped PLGA microparticles with internal pores fabricated by simple O/W emulsion, Chem. Commun. (Camb.) 46 (2010) 7433-7435.

[33] Z. Pan, J. Ding, Poly(lactide-co-glycolide) porous scaffolds for tissue engineering and regenerative medicine, Interface Focus 2 (2012) 366-377.

[34] M. M. Farag, W. M. Abd-Allah, A. M. Ibrahim, Effect of gamma irradiation on drug releasing from nano-bioactive glass, Drug Deliv. Transl. Res. 5 (2015) 63-73.

[35] H. Maleki, A. A. Gharehaghaji, T. Toliyat, P. J. Dijkstra, Drug release behavior of electrospun twisted yarns as implantable medical devices, Biofabrication 8 (2016) 035019.

[36] S. Bohrey, V. Chourasiya, A. Pandey, Polymeric nanoparticles containing diazepam: preparation, optimization, characterization, in-vitro drug release and release kinetic study, Nano Converg. 3 (2016) 3.

[37] S. Nakamura, S. Kondo, A. Mohri, T. Sakamoto, H. Yuasa, Preparation of Controlled-Release Particles Based on Spherical Porous Silica Used as the Drug Carrier by the Dry Coating Method, AAPS Pharm. Sci. Tech. 19 (2018) 1493-1499.

[38] A. Göpferich, Mechanisms of polymer degradation and erosion, Biomaterials 17 (1996) 103-114.

[39] R. Wada, S. H. Hyon, Y. Ikada, Kinetics of diffusion-mediated drug release enhanced by

matrix degradation, J. Control. Release 37 (1995) 151-160.

[40] J. Siepmann, A. Göpferich, Mathematical modeling of bioerodible, polymeric drug delivery systems, Adv. Drug Deliv. Rev. 48 (2001) 229-247.

[41] P. Fattahi, A. Borhan, M. R. Abidian, Microencapsulation of chemotherapeutics into monodisperse and tunable biodegradable polymers via electrified liquid jets: control of size, shape, and drug release, Adv. Mater. 25 (2013) 4555-4560.

[42] F. M. Chen, H. Lu, L. A. Wu, L. N. Gao, Y. An, J. Zhang, Surface-engineering of glycidyl methacrylated dextran/gelatin microcapsules with thermo-responsive poly(N-isopropylacrylamide) gates for controlled delivery of stromal cell-derived factor-1α, Biomaterials 34 (2013) 6515-6527.

Table 1. Correlation coefficients and release rate constants for different models

	Zero order		First order		Higuchi		Korsmeyer-peppas		
	K	R^2	K	R^2	K	R^2	K	n	R^2
MB	1.38	0.859	0.0243	0.959	14.9	0.940	6.35	0.659	0.920
NR	1.20	0.850	0.0349	0.995	13.2	0.963	9.90	0.543	0.952

Captions:

Figure 1. Schematic illustration of glass-capillary microfluidic device for generating water-in-oil-in-water (W/O/W) emulsion droplets. The orifice diameter of the innermost phase of the device (D_o) was 100 μm, and the diameter of the collection tube tip of the device was 300 μm. The inner channel size of the square tube was 1mm x 1mm; Q_i, Q_m and Q_o: the volume flow rates of fluid flow of the innermost water phase (Q_i = 1 mL/h), the middle oil phase (Q_m = 2 mL/h) and the outermost water phase (Q_o = 6 mL/h).

Figure 2. Schematic illustration of forming HA injectable scaffold.

Figure 3. Morphology of PLGA microspheres. Field-emission scanning electron micrograph (A) and size distribution (B) of PLGA microspheres; Three-dimensional overlay (C) of confocal scanning laser microscopy images of PLGA (D and E); (F) Cross-sectional morphology of PLGA microspheres.

Figure 4. In vitro release profiles of NR and MB from PLGA microspheres in the PBS solution (pH=7.4, 10% isopropanol，0.1% Tween 80) at 37°C. Date are presented as mean ± SD (standard deviation), n=6. ●MB, ■NR

Figure 5. Gross evaluation of the repaired tissue. (A) Macroscopic observation of the repaired tissues at 8 and 12 weeks. ICRS macroscopic scores of the regenerated tissue at 8 (B) and 12 (C) weeks. Bar scales: 3.5cm. Data are presented as mean ± SD (n = 3, *p < 0.05, **p < 0.01, ***p < 0.001).

Figure 6. Histology of the repaired tissues and microscopic evaluation. (A) H&E staining of the repaired tissue at 8 and 12 weeks. White arrows indicate the interface between the repaired tissue and

adjacent normal cartilage. H&E staining of high magnification of the repaired tissue at the central area (B) of the defect, and interface (C) between normal tissue and defect at 8 and 12 weeks, respectively. ICRS visual histological scores of the regenerated tissue at (D) 8 and (E) 12 weeks. Bar scales: 1000μm. Data are presented as mean ± SD (n = 3; **p < 0.01, ***p < 0.001).

Figure 7. TBO staining of the repaired tissues at 8 and 12 weeks. (Bar scale: 1000 μm).

Figure 8. Immunohistochemical staining of COL II of the repaired tissues at 8 and 12 weeks. (Bar scale: 1000 μm).

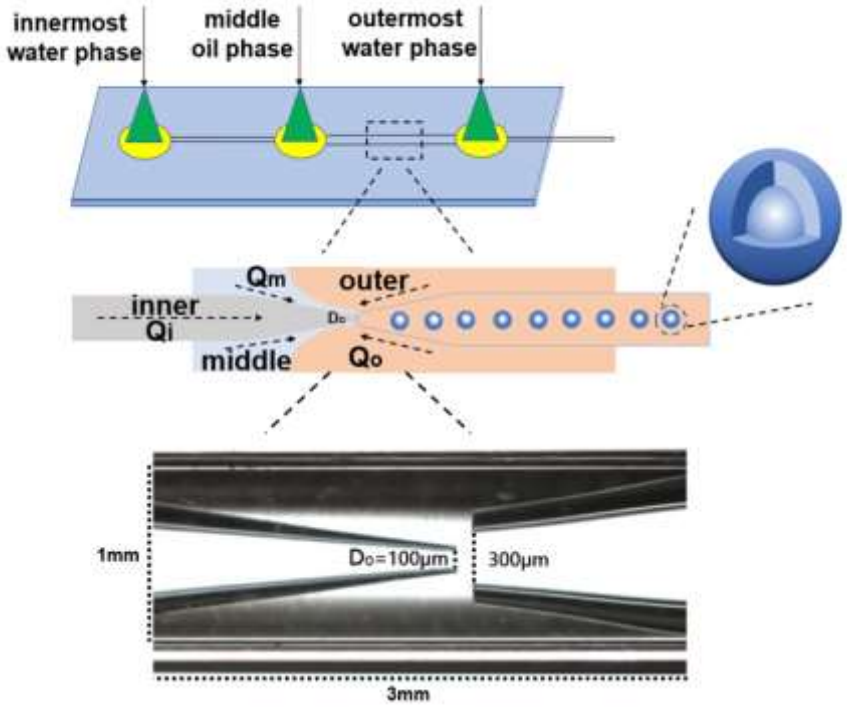
innermost
water phase
middle
oil phase
outermost
water phase
Qm
outer
inner
Qi
middle
Qo
1mm
Do=100μm
300μm
3mm

Figure 1

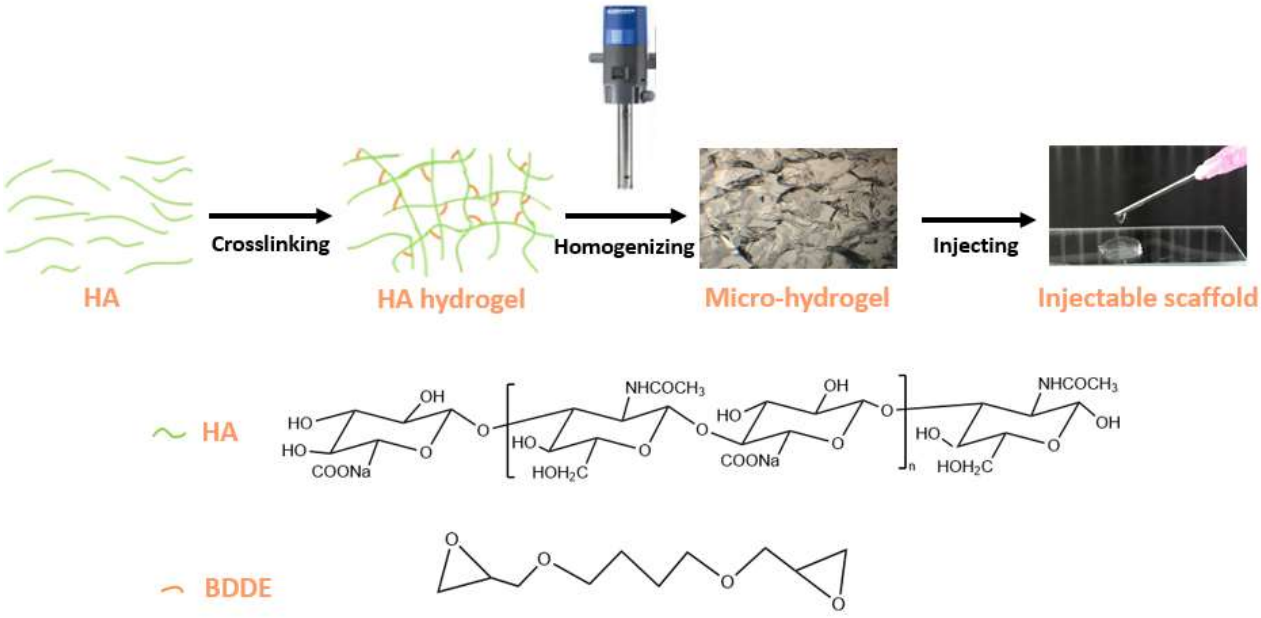
Crosslinking
Homogenizing
Injecting
HA
HA hydrogel
Micro-hydrogel
Injectable scaffold
HA
BDDE

Figure 2

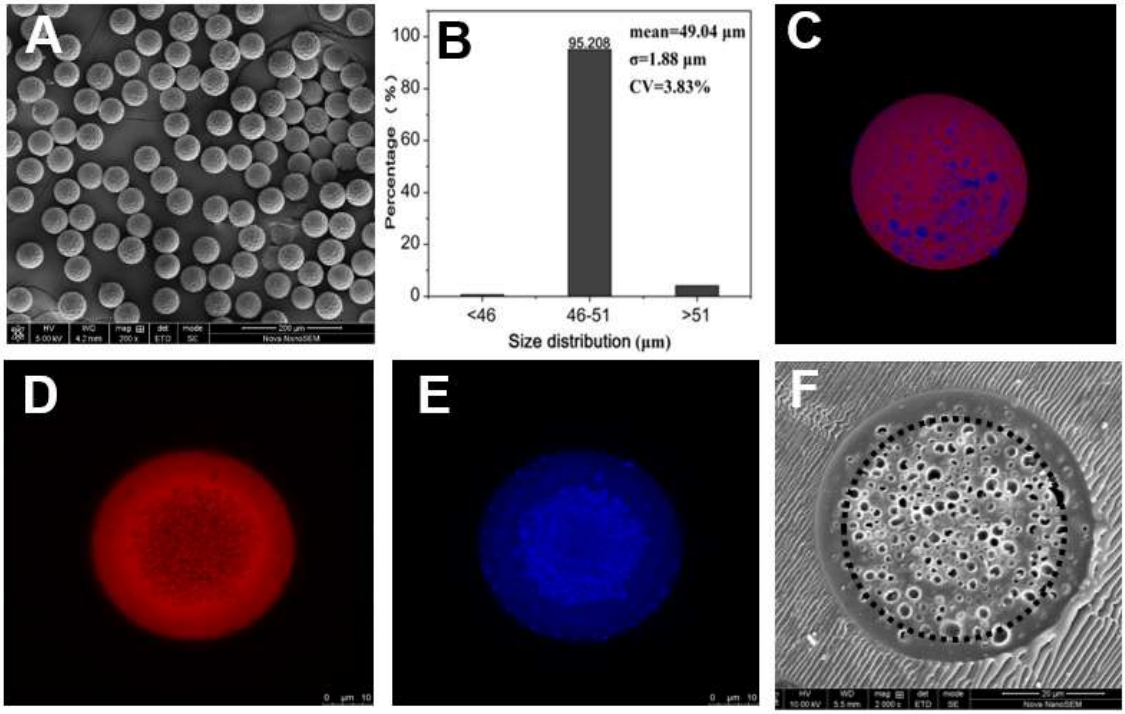
A
B
mean=49.04 μm
σ=1.88 μm
CV=3.83%
95.208
Percentage (%)
100
80
60
40
20
0
<46
46-51
>51
Size distribution (μm)
C
D
E
F

Figure 3

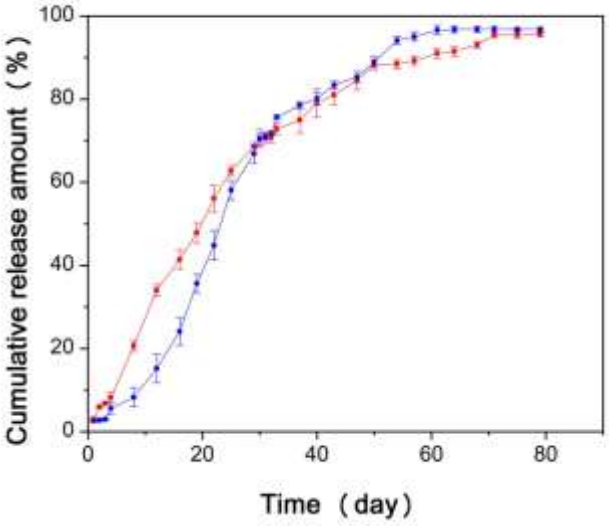

Figure 4

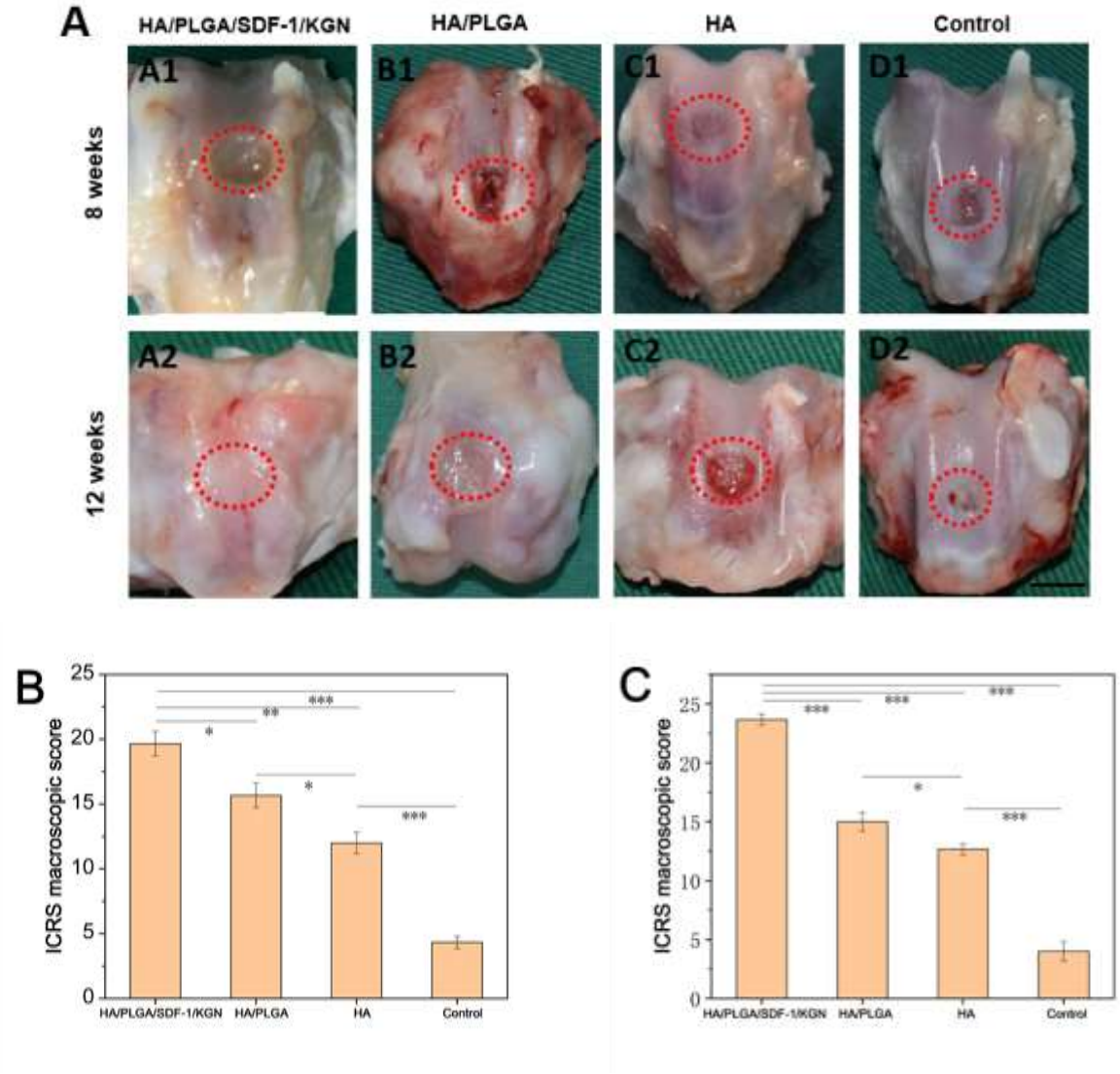
A
HA/PLGA/SDF-1/KGN
HA/PLGA
HA
Control
8 weeks
12 weeks
A1
B1
C1
D1
A2
B2
C2
D2
B
ICRS macroscopic score
HA/PLGA/SDF-1/KGN
HA/PLGA
HA
Control
C
ICRS macroscopic score
HA/PLGA/SDF-1/KGN
HA/PLGA
HA
Control

Figure 5.

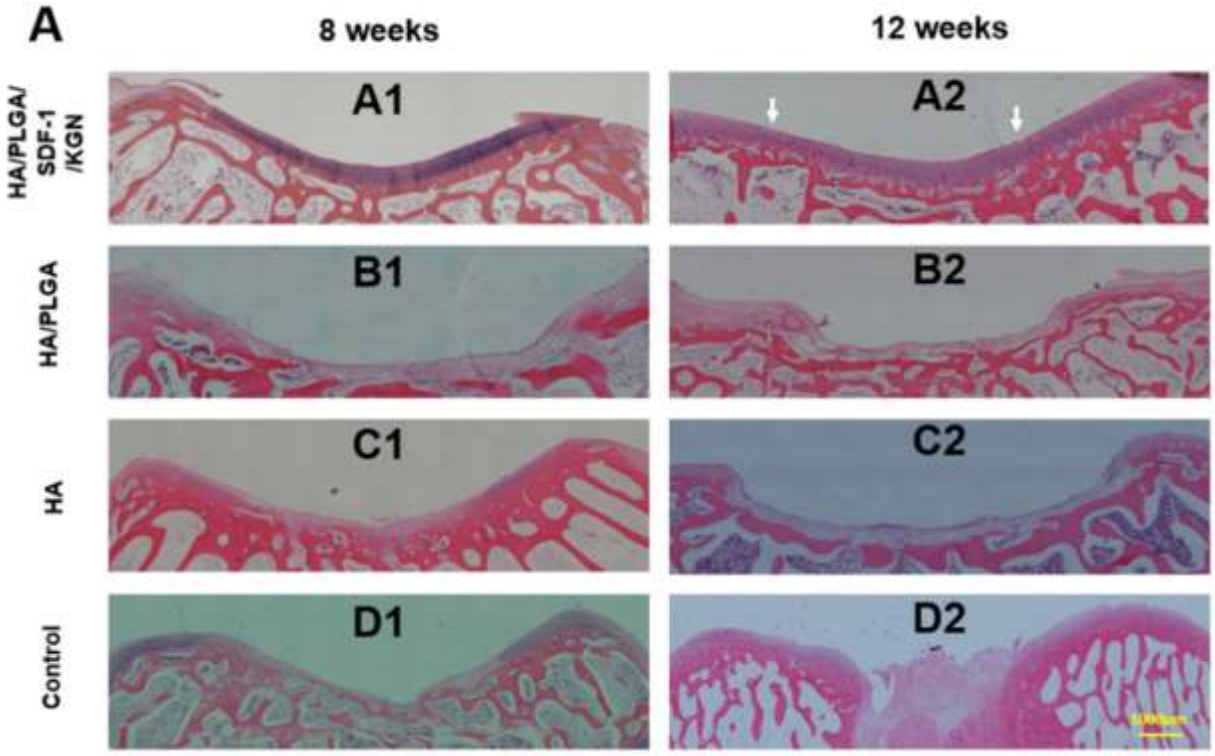
A
8 weeks
12 weeks
HA/PLGA/ SDF-1 /KGN
A1
A2
HA/PLGA
B1
B2
HA
C1
C2
Control
D1
D2

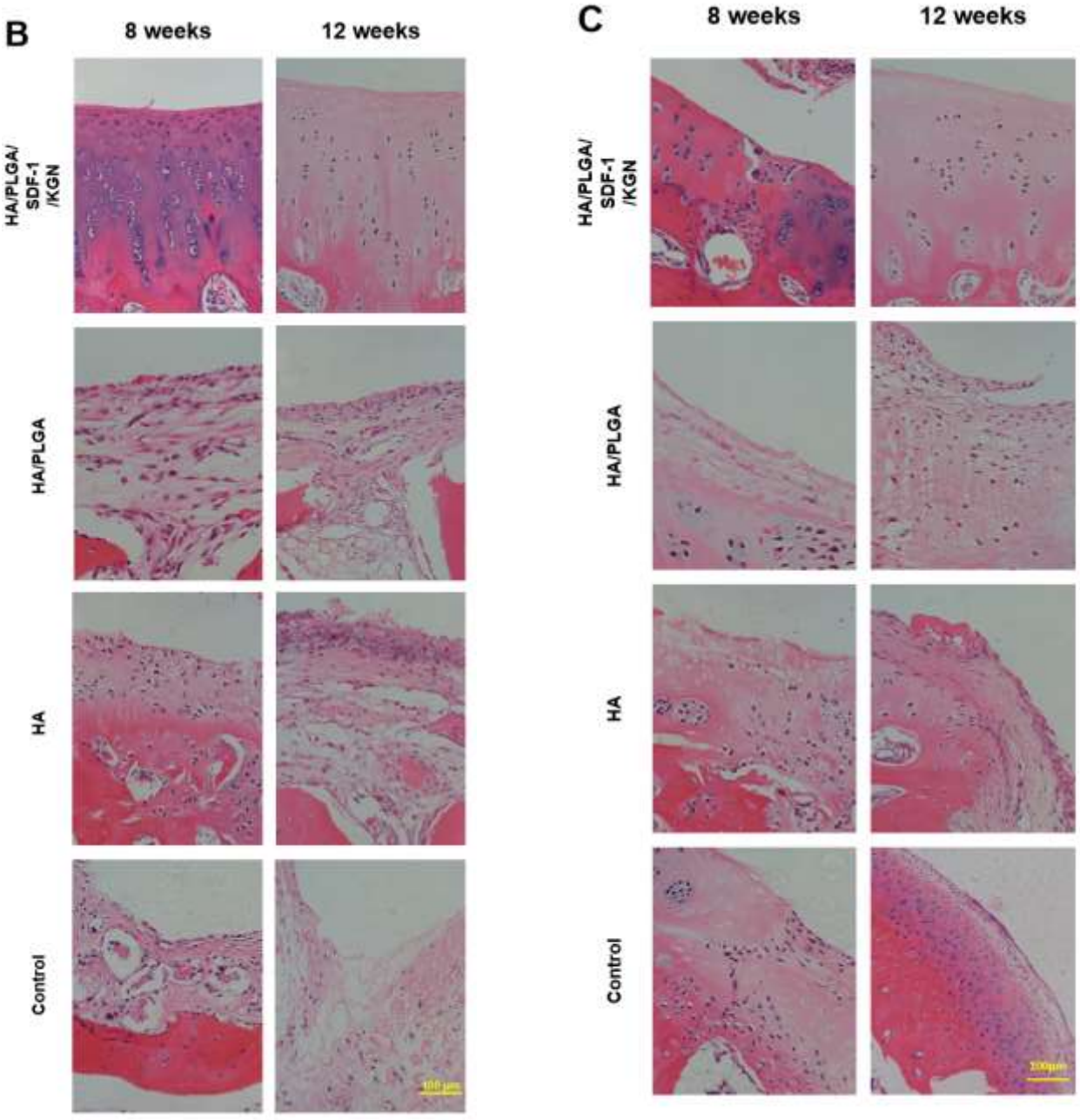
B
8 weeks
12 weeks
HA/PLGA/
SDF-1
/KGN
HA/PLGA
HA
Control
C
8 weeks
12 weeks
HA/PLGA/
SDF-1
/KGN
HA/PLGA
HA
Control

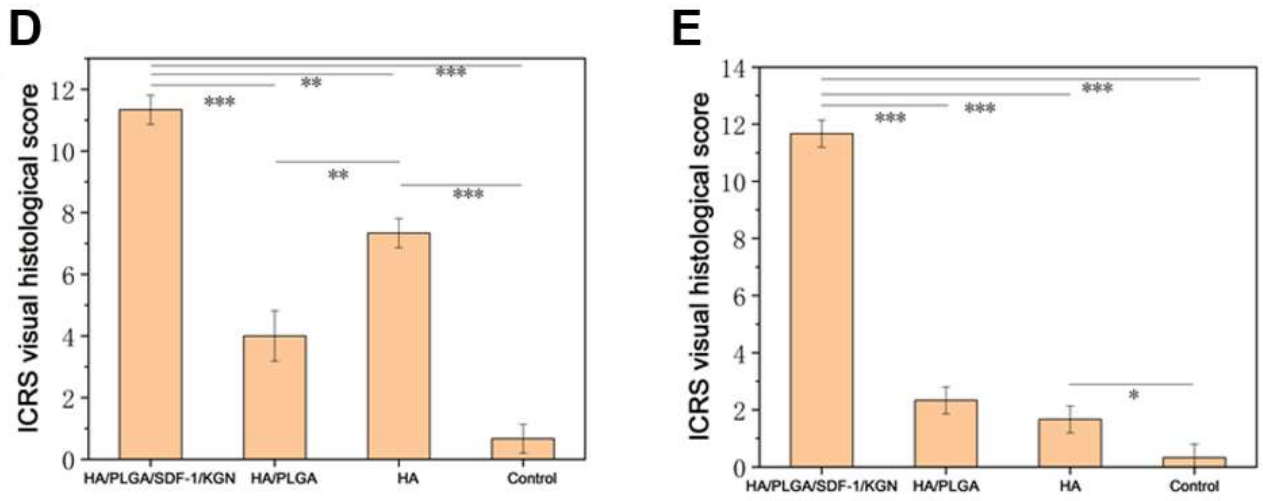
D
ICRS visual histological score
0
2
4
6
8
10
12
***
**
***
**
***
HA/PLGA/SDF-1/KGN
HA/PLGA
HA
Control
E
ICRS visual histological score
0
2
4
6
8
10
12
14
***
***
***
*
HA/PLGA/SDF-1/KGN
HA/PLGA
HA
Control

Figure 6

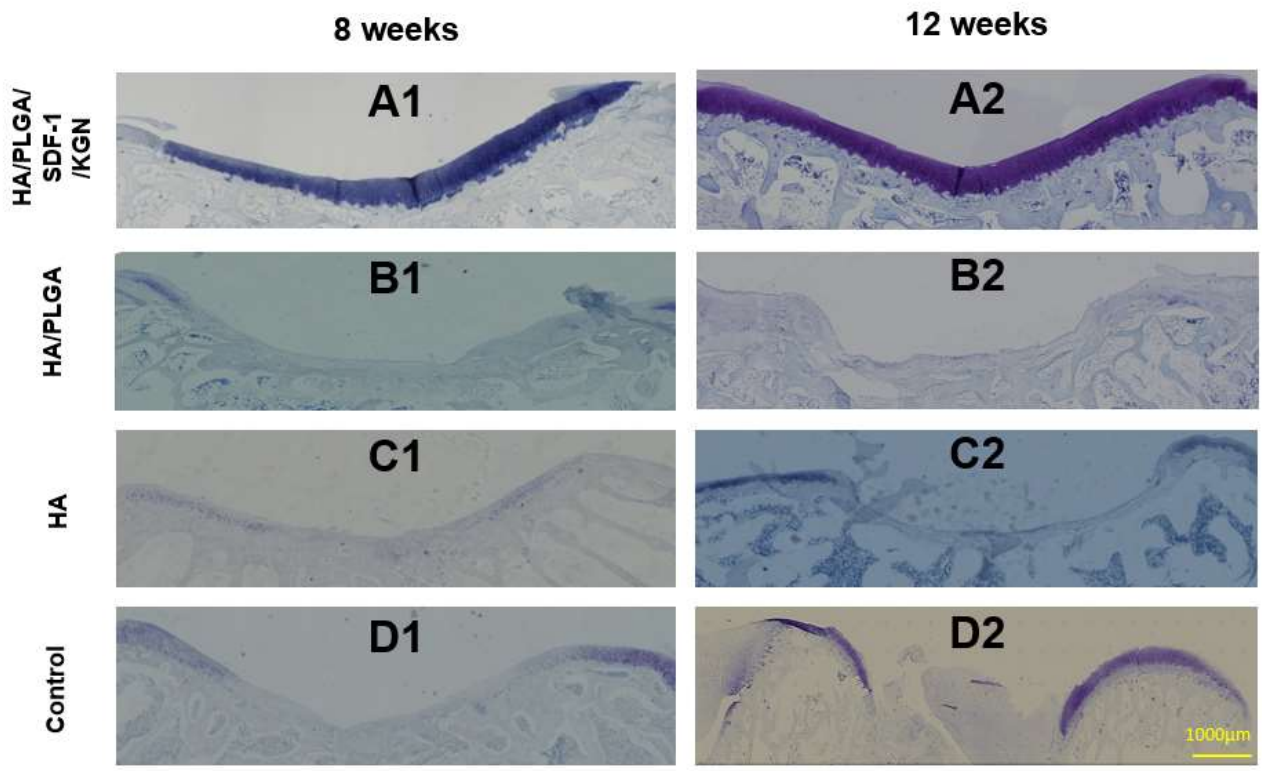
8 weeks
12 weeks
HA/PLGA/ SDF-1 /KGN
HA/PLGA
HA
Control
A1
A2
B1
B2
C1
C2
D1
D2
1000μm

Figure 7

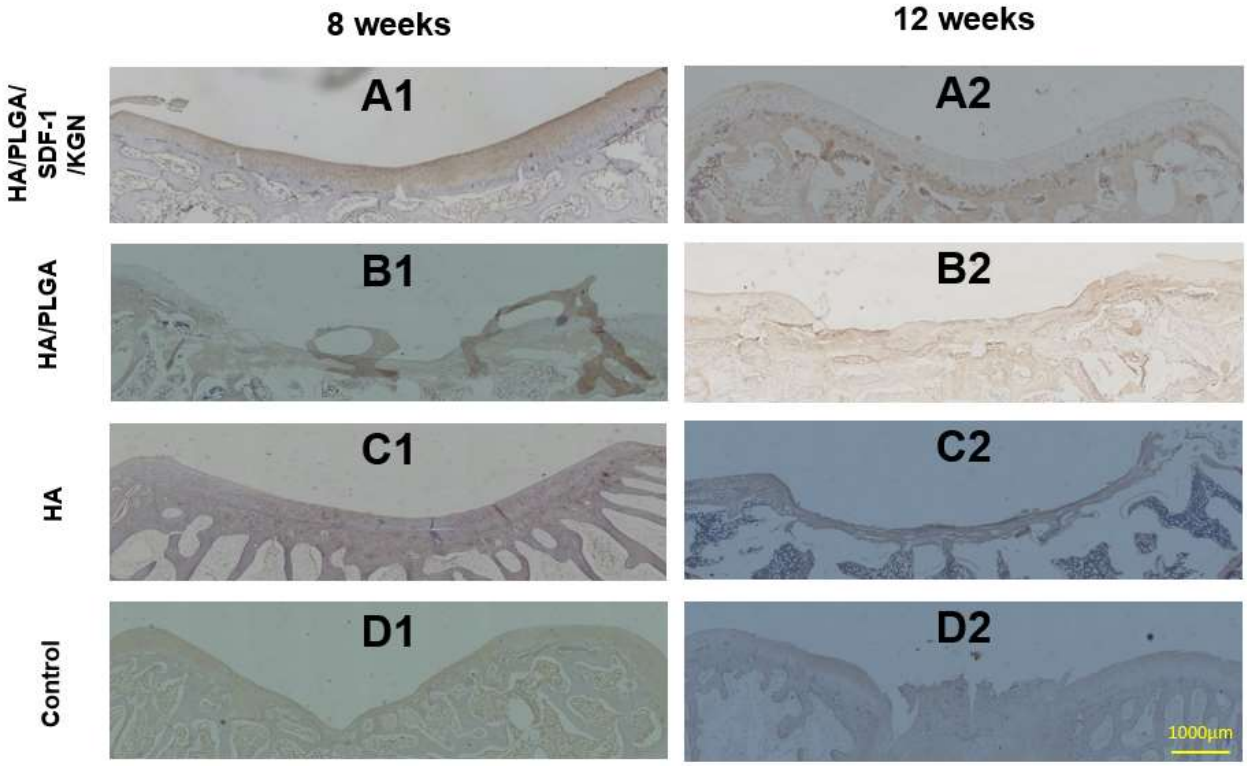
8 weeks
12 weeks
HA/PLGA/ SDF-1 /KGN
HA/PLGA
HA
Control
A1
A2
B1
B2
C1
C2
D1
D2
1000μm

Figure 8